TECHNICAL NOTES 8

GRINDING

R. P. King

8.1 Grinding

8.1.1 Grinding action

Industrial grinding machines used in the mineral processing industries are mostly of the tumbling mill type. These mills exist in a variety of types - rod, ball, pebble autogenous and semi-autogenous. The grinding action is induced by relative motion between the particles of media - the rods, balls or pebbles. This motion can be characterized as collision with breakage induced primarily by impact or as rolling with breakage induced primarily by crushing and attrition. In autogenous grinding machines fracture of the media particles also occurs by both impact (self breakage) and attrition.

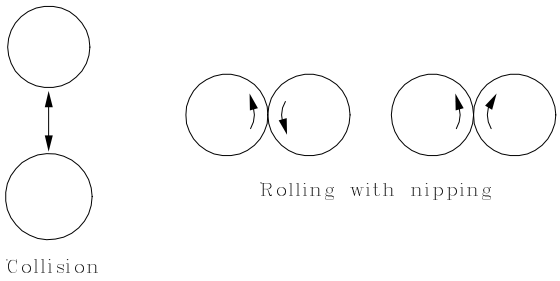

Figure 8.1 Different types of grinding action by the grinding media.

The relative motion of the media is determined by the tumbling action which in turn is quite strongly influenced by the liners and lifters that are always fixed inside the shell of the mill. Liners and lifters have two main purposes:

1. Liners protect the outer shell of the mill from wear - liners are renewable.
2. Lifters prevent slipping between the medium and slurry charge in the mill and the mill shell. Slippage will consume energy wastefully but more importantly it will reduce the ability of the mill shell to transmit energy to the tumbling charge. This energy is required to cause grinding of the material in the mill. The shape and dimensions of the lifters control the tumbling action of the media.

The tumbling action is difficult to describe accurately but certain regions in the mill can be characterized in terms of the basic pattern of motion of material in the mill.

The motion of an individual ball in the charge is complicated in practice and it is not possible to calculate the path taken by a particular particle during station of the charge. However the general pattern of the motion of the media can be simulated by discrete element methods which provide valuable information about the dynamic conditions inside the mill.

Some of the terms that are often used to describe the motion of the media in a tumbling mill are shown in Figure 8.2

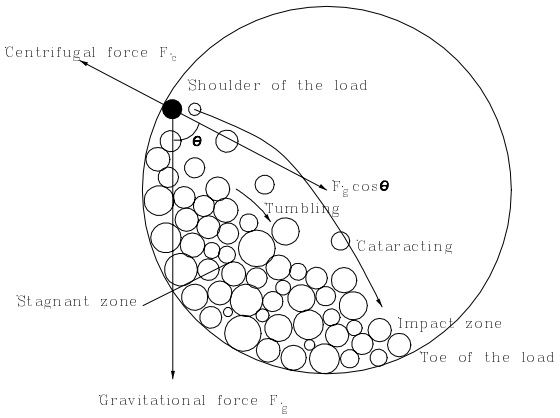

Figure 8.2 Media motion in the tumbling mill.

8.1.2 Critical speed of rotation

The force balance on a particle against the wall is given by

Centrifugal force outward

$$F_c = m_p \omega^2 \frac{D_m}{2} \tag{8.1}$$

ω is the angular velocity, m_p is the mass of any particle (media or charge) in the mill and D_m is the diameter of the mill inside the liners.

Gravitational force

$$F_g = m_p g \tag{8.2}$$

The particle will remain against the wall if these two forces are in balance ie.

$$F_c = F_g \cos\theta \tag{8.3}$$

where θ is shown in Figure 8.2
Thus a particle will separate from the wall at the point where

$$\cos\theta = \frac{F_c}{F_g} \tag{8.4}$$

The critical speed of the mill, ω_c, is defined as the speed at which a single ball will just remain against the wall for a full cycle. At the top of the cycle θ=0 and

$$F_c = F_g \tag{8.5}$$

$$m_p \frac{\omega_c^2 D_m}{2} = m_p g \tag{8.6}$$

$$\omega_c = \left(\frac{2g}{D_m} \right)^{1/2} \tag{8.7}$$

The critical speed is usually expressed in terms of the number of revolutions per second

$$N_c = \frac{\omega_c}{2\pi} = \frac{1}{2\pi}\left(\frac{2g}{D_m} \right)^{1/2} = \frac{(2\times 9.81)^{1/2}}{2\pi D_m^{1/2}}$$

$$= \frac{0.705}{D_m^{1/2}} \quad \text{revs/sec} \tag{8.8}$$

$$= \frac{42.3}{D_m^{1/2}} \quad \text{revs/min}$$

The liner profile and the stickiness of the pulp in the mill can have a significant effect on the actual critical velocity.

Mills usually operate in the range 65 - 82% of critical but values as high as 90% are sometimes used.

A crucial parameter that defines the performance of a mill is the energy consumption. The power supplied to the mill is used primarily to lift the load (medium and charge). Additional power is required to keep the mill rotating.

8.1.3 Power drawn by ball, semi-autogenous and autogenous mills

A simplified picture of the mill load is shown in Figure 8.3 Ad this can be used to establish the essential features of a model for mill power.

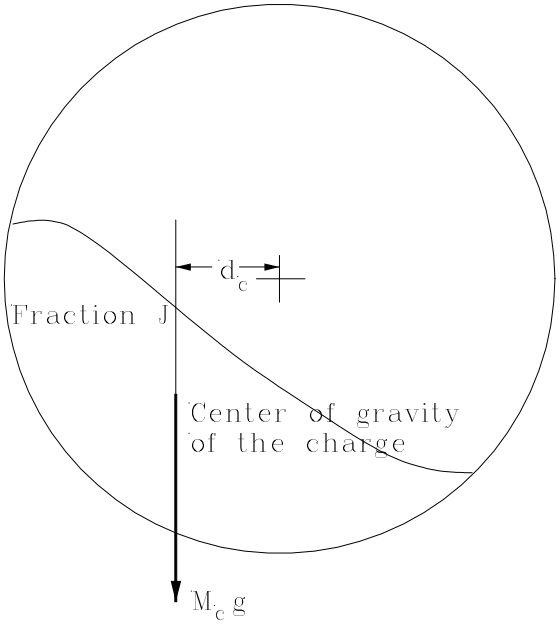

Figure 8.3 Simplified calculation of the torque required to turn a mill.

The torque required to turn the mill is given by

$$\text{Torque} = T = M_c g d_c + T_f \tag{8.9}$$

Where M_c is the total mass of the charge in the mill and T_f is the torque required to overcome friction.

$$\text{Power} = 2\pi NT \tag{8.10}$$

For mills of different diameter but running at the same fraction of critical speed and having the same fractional filling

$$\begin{aligned} \text{Net power} &= 2\pi N M_c d_c \\ &= \alpha N_c M_c d_c \\ &= \alpha \frac{1}{D_m^{0.5}} L D_m^2 D_m \\ &= \alpha L D_m^{2.5} \end{aligned} \tag{8.11}$$

The exponent 2.5 on D_m has been variously reported to have values as low as 2.3 and as high as 3.0.

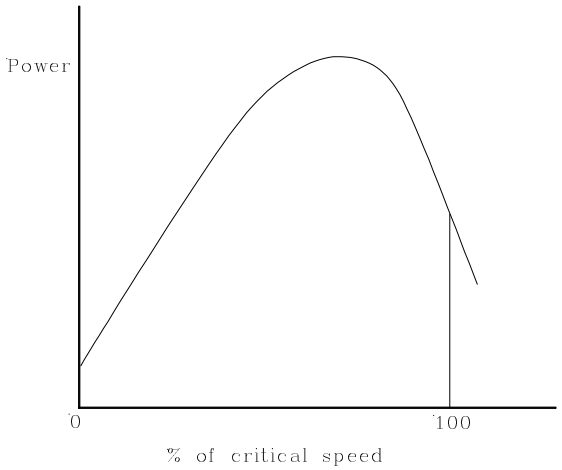

Figure 8.4 The effect of mill speed on the power drawn by a rotating mill.

The effect of varying mill speed on the power drawn by the mill is shown graphically in Figure 8.4

The speed of rotation of the mill influences the power draft through two effects: the value of *N* and the shift in the center of gravity with speed. The center of gravity first starts to shift to the left as the speed of rotation increases but as critical speed is reached the center of gravity moves towards the center of the mill as more and more of the material is held against the shell throughout the cycle. Since critical speed is larger at smaller radii the centrifuging layer gets thicker and thicker as the speed increases until the entire charge is centrifuging and the net power draw is zero.

The effect of mill charge is primarily through the shifting of the center of gravity and the mass of the charge. As the charge increases the center of gravity moves inward. The power draft is more or less symmetrical about the 50% value.

A simple equation for calculating net power draft is

$$P = 2.00\ \varphi_c D_m^{2.5} L\, K_l \qquad \text{kW} \qquad (8.12)$$

K_l is the loading factor which can be obtained from Figures 8.5 for the popular mill types. φ_c is the mill speed measured as a fraction of the critical speed.

More reliable models for the prediction of the power drawn by ball, semi-autogenous and fully autogenous mills have been developed by Morrell and by Austin. (Morrell, S. Power draw of wet tumbling mills and its relationship to charge dynamics - Part 2: An empirical approach to modeling of mill power draw. *Trans. Instn. Mining. Metall. (Sect C:Mineral Processing Extr Metall.)* **105**, January-April 1996 ppC54-C62. Austin LG A mill power equation for SAG mills. *Minerals and Metallurgical Processing.* Feb 1990 pp57-62.

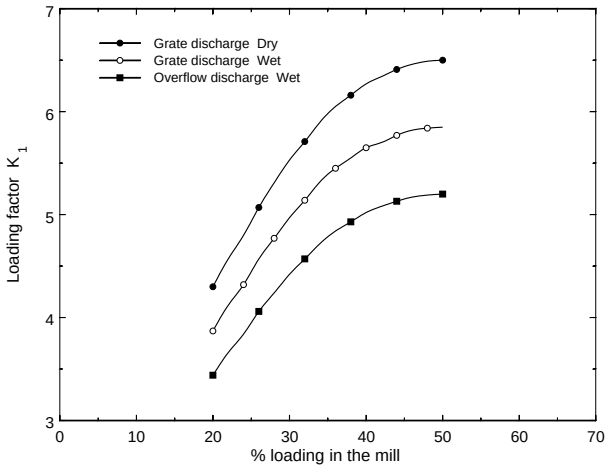

Figure 8.5 Effect of mill filling on power draft for ball mills. The data is taken from Rexnord Process Machinery Reference Manual, Rexnord Process Machinery Division, Milwaukee, 1976

$$\text{Gross power} = \text{No-load power} + \text{Net power drawn by the charge} \qquad (8.13)$$

The net power is calculated from

$$\text{Net power} = KD^{2.5} L_e \rho_c \alpha \delta \qquad \text{Watts} \qquad (8.14)$$

In equation 8.14, D is the diameter inside the mill liners and L_e is the effective length of the mill including the conical ends. ρ_c is the specific gravity of the charge and α and δ are factors that account for the fractional filling and the speed of rotation respectively. *K* is a calibration constant that varies with the type of discharge. For overflow mills $K = 7.98$ and for grate mills $K = 9.10$. This difference is ascribed to the presence of a pool of slurry that is present on the bottom of overflow-discharge mills but not to the same extent in grate-discharge mills. This pool is situated more or less symmetrically with respect to the axis of the mill and therefore does not draw significant power. Austin recommends $K = 10.6$ for overflow semi-autogenous mills. A value of $K = 9.32$ makes Austin's formula agree with Morrell's data as shown in Figure 8.7

The no-load power accounts for all frictional and mechanical losses in the drive system of the mill and can be calculated from

$$\text{No-load power} = 1.68D^{2.05}[\varphi_c(0.667L_d + L)]^{0.82} \quad \text{kW} \tag{8.15}$$

L_d is the mean length of the conical ends and is calculated as half the difference between the center-line length of the mill and the length of the cylindrical section.

The geometry of a mill with conical ends is shown in Figure 8.6. The total volume inside the mill is given by

$$V_m = \frac{\pi}{4}D_m^2 L\left(1 + \frac{2(L_c - L)}{L}\,\frac{1-(D_t/D_m)^3}{1-D_t/D_m}\right) \tag{8.16}$$

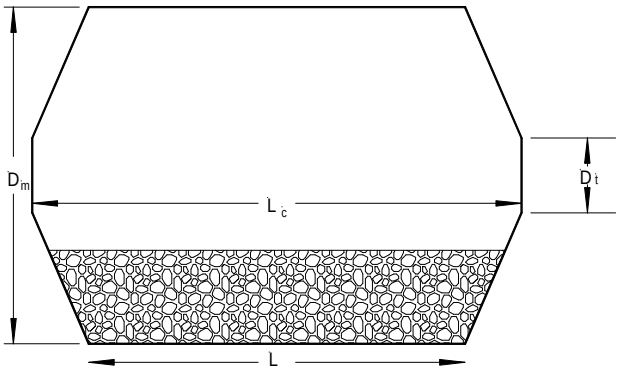

Figure 8.6 Geometry of a mill with cylindrical ends. All dimensions are inside liners. L_c = centerline length. L = belly length. D_m = mill diameter. D_t = trunnion diameter.

The density of the charge must account for all of the material in the mill including the media which may be steel balls in a ball mill, or large lumps of ore in an autogenous mill or a mixture in a semi-autogenous mill, as well as the slurry that makes up the operating charge. Let J_t be the fraction of the mill volume that is occupied by the total charge, J_b the fraction of the mill volume that is occupied by steel balls and E the voidage of the balls and media. U is the fraction of the voidage that is filled by slurry. φ_v is the volume fraction of solids in the slurry. Let V_B be the volume of steel balls in the mill, V_{Med} be the volume of autogenous media and V_S the volume of slurry.

$$\begin{aligned} V_B &= J_b(1-E)V_m \\ V_S &= J_t UEV_m \\ V_{Med} &= (J_t - J_b)(1-E)V_m \end{aligned} \tag{8.17}$$

The charge density is calculated from

$$\rho_c = \frac{V_B\rho_b + V_{Med}\rho_m + V_S(1-\varphi_v)1000 + V_S\varphi_v\rho_0}{J_t} \tag{8.18}$$

where ρ_b is the density of the balls and ρ_m the density of the media. The effective length of the mill is dependent on the load and is calculated from

$$L_e = L\left(1 + 2.28J_t(1-J_t)\frac{L_d}{L}\right) \tag{8.19}$$

according to Morrell and from

$$L_e = L(1 + f_3)$$

$$f_3 = \frac{0.092}{J_t(1 - 1.03J_t)}\left(\frac{L_d}{L(1 - D_t/D)}\left[\left(\frac{0.625}{0.5 - J_t}\right)^{0.1} - \left(\frac{0.625}{0.5 - J_t}\right)^{-4}\right]\right) \qquad (8.20)$$

according to Austin.

The functions α and δ account for the effects of mill filling and rotation speed respectively. However each of these factors is a function of both mill filling and rotation speed

$$\alpha = \frac{J_t(\omega - J_t)}{\omega^2} \qquad (8.21)$$

$$\omega = 2(2.986\varphi_c - 2.213\varphi_c^2 - 0.4927)$$

and

$$\delta = \varphi_c\left(1 - [1 - \varphi_{max}]\exp(-19.42(\varphi_{max} - \varphi_c))\right) \qquad (8.22)$$

$$\varphi_{max} = 0.954 - 0.135J_t$$

Austin recommends the following forms for the factors α and δ

$$\alpha = J_t(1 - 1.03J_t)$$

$$\delta = \varphi_c\left(1 - \frac{0.1}{2^{9 - 10\varphi_c}}\right) \qquad (8.23)$$

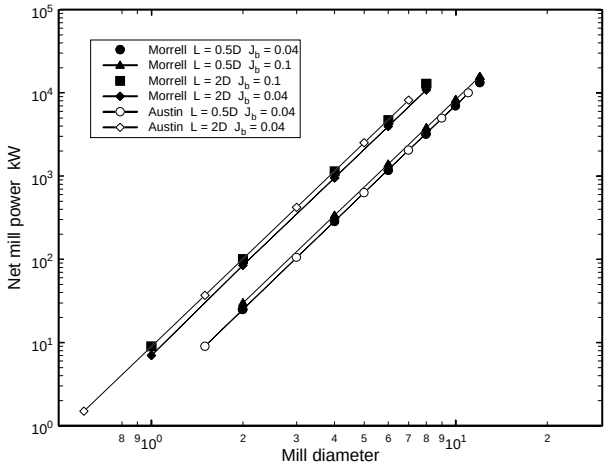

Figure 8.7 Variation of net power drawn by semi-autogenous mills calculated using the formulas of Austin and Morrell. Mill conditions used: J_t = 0.35, E = 0.4, U = 1.0, φ_c = 0.72, D_o = 0.1D, L_d = 0.25D, ρ_B = 7800, ρ_O = 2750, φ_v = 0.459

The formulas proposed by Austin and Morrell give substantially the same estimates of the net power that is drawn by the mill. Some typical cases are shown in Figure 8.8. Austin's formula gives slightly higher values than Morrell's for mills that have length equal to about twice the diameter.

8.1.4 Power drawn by rod mills

The power drawn by a rod mill is given by

$$P = 1.752D^{0.33}(6.3 - 5.4V_p)\varphi_c \qquad \text{kW hr/tonne of rods charged} \qquad (8.24)$$

where V_p = fraction of the mill volume that is loaded with rods. Rod mills operate typically at φ_c between 0.64 and 0.75 with larger diameter mills running at the lower end and smaller mills at the upper end. Typical rod loads are 35% to 45% of mill volume and rod bulk densities range from about 5400 kg/m^3 to 6400 kg/m^3.
(Rowlands CA and Kjos DM. Rod and ball mills in Mular AL and Bhappu R B Editors Mineral Processing Plant Design 2nd edition. SME Littleton CO 1980 Chapter 12 p239)

8.1.5 The impact energy spectrum in a mill

The energy that is required to break the material in the mill comes from the rotational energy that is supplied by the drive motor. This energy is converted to kinetic and potential energy of the grinding media. The media particles are lifted in the ascending portion of the mill and they fall and tumble over the charge causing impacts that crush the individual particles of the charge. The overall delivery of energy to sustain the breakage process is considered to be made up of a very large number of individual impact or crushing events. Each impact event is considered to deliver a finite amount of energy to the charge which in turn is distributed unequally to each particle that is in the neighborhood of the impacting media particles and which can therefore receive a fraction of the energy that is dissipated in the impact event. Not all impacts are alike. Some will be tremendously energetic such as the impact caused by a steel ball falling in free flight over several meters. Others will result from comparatively gentle interaction between media pieces as they move relative to each other with only little relative motion. It is possible to calculate the distribution of impact energies using discrete element methods to simulate the motion of the media particles including all the many collisions in an operating mill. The distribution of impact energies is called the impact energy spectrum of the mill and this distribution function ultimately determines the kinetics of the comminution process in the mill.

8.1.6 Kinetics of Breakage

The process engineering of milling circuits is intimately linked with the kinetic mechanisms that govern the rate at which material is broken in a comminution machine.

In any region of a comminution machine the rate at which material of a particular size is being broken is a strong function of the amount of that size of material present. The rate of breakage varies with size.

It is usual to use discrete size classes which provides an adequate approximation for practical computation.

Rate of breakage of material out of size class $i = k_i M m_i$.
k_i is called the specific rate of breakage. It is also called the selection function in older texts.
Note that k_i is a function of the representative size in the class.

Material breaking out of class i distributes itself over all other classes according to the breakage function which is specific to the comminution operation and the material being broken.

It is common practice to normalise the breakage function to the lower mesh size of the interval so that breakage means breakage out of a size class. If the breakage function is described by the standard form.

$$B(x;y) = K\left(\frac{x}{y}\right)^{n_1} + (1-K)\left(\frac{x}{y}\right)^{n_2} \qquad (8.25)$$

and

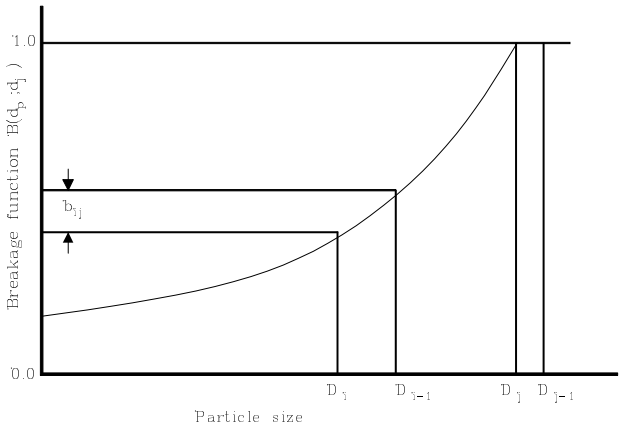

Figure 8.8 The breakage function used for the description of milling operations in rotating mills. Compare with the equivalent diagram for crushing machines (Figure 5.14)

$$b_{ij} = B(D_{i-1}; D_j) - B(D_i; D_j)$$
$$b_{jj} = 0 \qquad (8.26)$$

The relationship between the cumulative breakage function and b_{ij} is shown in Figure (8.8). The breakage function has the value 1.0 at the lower boundary of the parent size interval. This reflects the convention that breakage is assumed to occur only when material leaves the parent size interval. The differences between equation (8.26) and the equivalent expressions for crushing machines (5.39) should be noted.

K represents the fraction of fines that are produced in a single fracture event. It is in general a function of the parent size so that

$$K = K_1\left(\frac{d_{p_i}}{d_{p_1}}\right)^{-n_3} \qquad (8.27)$$

If normalisation is satisfactory and if a strictly geometric progression is used for the mess size then B_{ij} is a function only of the difference *i-j*. For example if a root 2 series is used for the size classes.

$$\frac{D_i}{D_j} = \frac{D_i}{(\sqrt{2})^{i-j}D_i} = (\sqrt{2})^{j-i} \qquad (8.28)$$

$$b_{ij} = K\left(\frac{D_{i-1}}{D_j}\right)^{n_1} + (1-K)\left(\frac{D_{i-1}}{D_j}\right)^{n_2} - K\left(\frac{D_i}{D_j}\right)^{n_1} + (1-K)\left(\frac{D_i}{D_j}\right)^{n_2} \qquad (8.29)$$

$$\begin{aligned} b_{ij} &= K\left[(\sqrt{2})^{n_1(j-i+1)} - (\sqrt{2})^{n_1(j-i)}\right] + (1-K)\left[(\sqrt{2})^{n_2(j-i+1)} - \sqrt{2}^{n_2(j-i)}\right] \\ &= K(\sqrt{2})^{n_1(j-i)}(\sqrt{2}-1) + (1-K)(\sqrt{2})^{n_2(j-i)}(\sqrt{2}-1) \\ &= 0.414K(\sqrt{2})^{n_1(j-i)} + 0.414(1-K)(\sqrt{2})^{n_2(j-i)} \end{aligned} \qquad (8.30)$$

8.2 The Continuous Mill.

Industrial grinding mills always process material continuously so that models must simulate continuous operation. Suitable models are developed in this section.

8.2.1 The population balance model for a perfectly mixed mill.

The equations that describe the size reduction process in a perfectly mixed ball mill can be derived directly from the master population balance equation that was developed in Chapter 2. However, the equation is simple enough to derive directly from a simple mass balance for material in any specific size class.

Define

p_i^F = fraction feed in size class i
p_i^P = fraction of product in size class i
m_i = fraction of mill contents in size class i
M = mass of material in the mill.
W = mass flowrate through the mill.

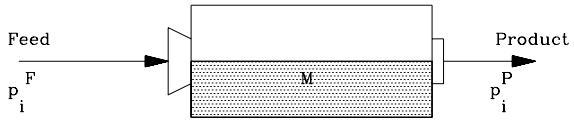

Figure 8.9 The perfectly mixed continuous mill

A mass balance on size class i is developed by noting that the contents of the mill receives material in size class i from the feed and from the breakage of material in the mill that is of size greater than size i. Material of size i is destroyed in the mill by fracture.

$$\begin{aligned} Wp_i^P &= Wp_i^F + M\sum_{j=1}^{i-1} b_{ij}k_j m_j - Mk_i m_i \\ p_i^P &= p_i^F + \tau\sum_{j=1}^{i-1} b_{ij}k_j m_j - k_i\tau m_i \end{aligned} \tag{8.31}$$

where $\tau=M/W$ is the average residence time of the material in the mill.
If the contents of the mill are assumed to be perfectly mixed $m_i=p_i^P$

$$\begin{aligned} p_i^P &= p_i^F + \sum_{j=1}^{i-1} b_{ij}k_j\tau p_j^P - k_i\tau p_i^P \\ p_i^P &= \frac{p_i^F + \sum_{j=i}^{i-1} b_{ij}k_j\tau p_j^P}{1+k_i\tau} \qquad \text{for all } i \end{aligned} \tag{8.32}$$

These can be solved by a straightforward recursion relationship starting with size class 1.

$$\begin{aligned} p_1^P &= \frac{p_1^F}{1+k_1\tau} \\ p_2^P &= \frac{p_2^F + b_{21}\tau k_1 p_1^P}{1+k_2\tau} \\ p_3^P &= \frac{p_3^F + b_{31}\tau k_1 p_1^P + b_{32}\tau k_2 p_2^P}{1+k_3\tau} \end{aligned} \tag{8.33}$$

etc.

8.2.2 The mill with post classification.

In practice the material in the mill does not have unrestricted ability to leave in the outlet stream. Larger

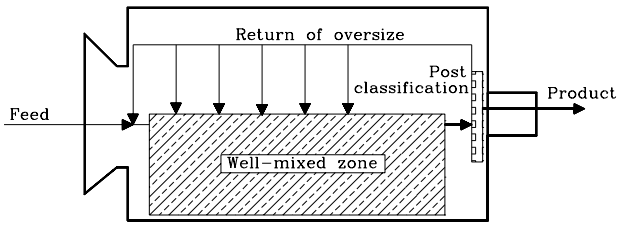

Figure 8.10 The classification mechanism at the mill discharge end recycles larger particles into the body of the mill.

particles are prevented from leaving by the discharge grate if one is present and even in overflow discharge mills, the larger particles do not readily move upward through the medium bed to the discharge. On the other hand very small particles move readily with the water and are discharged easily. Thus the discharge end of the mill behaves as a classifier which permits the selective discharge of smaller particles and recycles the larger particles back into the body of the mill. This is illustrated schematically in Figure (8.10). The operation of such a mill can be modeled as a perfectly mixed mill with post classification as shown in Figure (8.11).

Applying equation (8.32) to the perfectly mixed milling section

$$m_i = \frac{f_i' + \sum_{j=1}^{i-1} b_{ij} k_j \tau' m_j}{1 + \tau' k_i} \tag{8.34}$$

In this equation, τ' is the effective residence time in the mixed section of the mill

$$\tau' = \frac{M}{W(1+C)} = \frac{\tau}{(1+C)} \tag{8.35}$$

where C is the ratio of recirculation rate to feed rate.

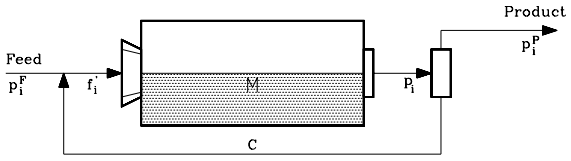

Figure 8.11 The perfectly mixed mill with post classification. The classification mechanism illustrated in Figure (8.10) is equivalent to a perfectly mixed mill with post classification.

A mass balance on size class i at the point where the post classified material re-enters the mill gives

$$(1+C) f_i' = c_i m_i (1+C) + p_i^F \tag{8.36}$$

where c_i is the classification constant for the particles of size i at the mill discharge.

Substituting the expression for f_i' into equation(8.32) gives, after some simplification,

$$m_i(1+C) = \frac{p_i^F + \sum_{j=1}^{i-1} b_{ij} k_j \tau' m_j (1+C)}{1 + \tau' k_i - c_i} \tag{8.37}$$

If a new variable $m_i^* = m_i(1+C)$ is defined , this equation takes a form identical to equation (8.32)

$$m_i^* = \frac{p_i^F + \sum_{j=1}^{i-1} b_{ij} k_j \tau' m_j^*}{1 + \tau' k_i - c_i} \tag{8.38}$$

This equation can be solved using the same recursive procedure as that used for (8.32) starting from the largest size.

The size distribution in the product can be obtained from the calculated values of m_i^* using the properties of the classifier.

$$p_i^P = (1-c_i)(1+C)m_i = (1-c_i)m_i^* \tag{8.39}$$

This solution is complicated a little because the modified residence time is not usually known. It can be calculated only after the size distribution in the mixed section has been evaluated. This requires an iterative solution for convenient implementation starting with an assumed value of τ' to calculate m_i^* from equation (8.38). C is calculated from

$$C = \sum_i c_i(1+C)m_i = \sum_i c_i m_i^* \tag{8.40}$$

and the assumed value for τ' can be checked using equation 8.35 and modified until convergence is obtained.

The actual residence time can be obtained from the load of solid in the mill and the mass flowrate of the solid through the mill or from a dynamic tracer experiment. It is usually easier to trace the liquid phase than the solid but the residence time of the liquid will be considerably shorter because of the holdback of the solid by the classsification mechanism of the discharge.

The precise form of the classification function can be determined by measuring the size distribution of the material in the mill contents and in the product stream

$$1-c_i = \frac{p_i^P}{(1+C)m_i} \tag{8.41}$$

The presence of post classification in a mill can be detected by noting the difference in particle size distribution between the mill contents and the discharged product. An example is shown in Figure (8.12)

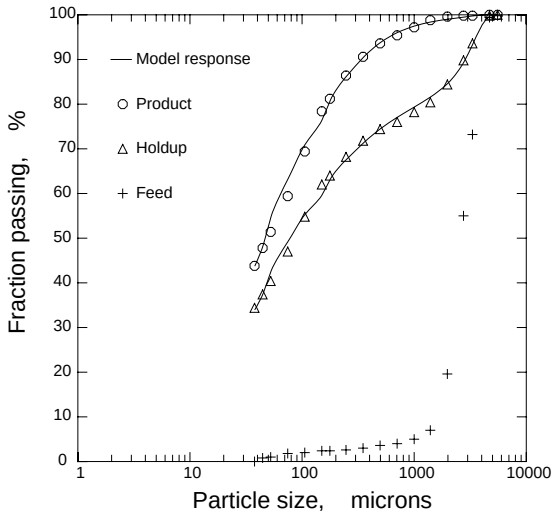

Figure 8.12 Experimentally determined particle-size distributions in the contents of the mill and the discharged product.

8.3 Mixing Characteristics of Operating Mills

In practice operating mills do not conform particularly well to the perfectly mixed pattern because there is considerable resistance to the transport of material, both solids and water, longitudinally along the mill. This type of behavior can be modeled quite well by several perfectly mixed segment in series with discharge from the last segment being restricted by a post classifier. The size distribution in the material that leaves each segment can be calculated by repeated application of equation

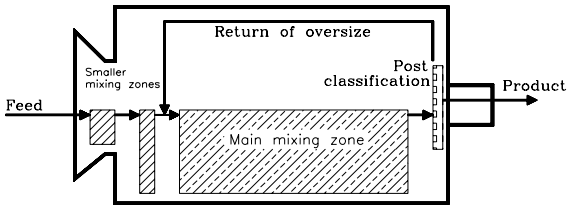

Figure 8.13 Schematic representation of the mill with three perfectly mixed segments of unequal size. Discharge from the last segment is restricted by a post classifier.

(8.32) successively to each mixed segment in turn. The product from the first segment becomes the feed to the next and so on down the mill. The number of mixed sections and their relative sizes can be determined from the residence-time distribution function in the mill. Residence distribution functions have been measured in a number of operating ball, pebble and autogenous mills and it is not unusual to find that three unequal perfectly mixed segments are adequate to describe the measured residence-time distribution functions. Usually the last segment is significantly larger than the other two. This is consistent with the behavior of a post classifier that holds up the larger particles at the discharge end of the mill which are then thrown quite far back into the body of the mill.

It has been suggested in the literature that a further refinement to the mixed-region model can be achieved by the use of a classification action between each pair of segments, but since it is impossible to make independently verifiable measurements of such interstage classifications, this refinement cannot be used effectively.

The structure of a mill with three perfectly-mixed segments with post classification on the last is illustrated in Figure (8.13).

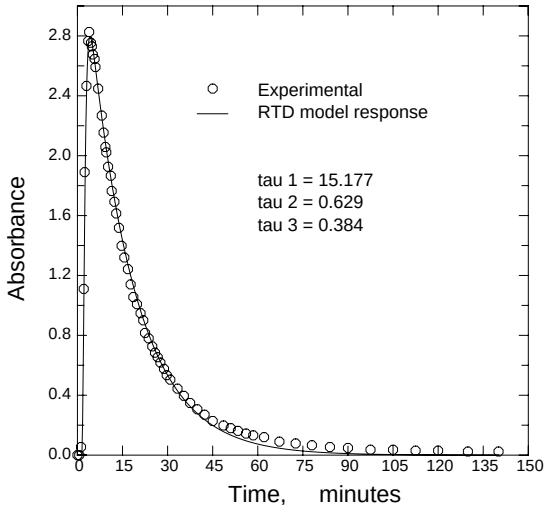

Figure 8.14 Residence time distribution function for the water in a continuous ball mill. The line shows the small-small-large segment model response to this data.

.

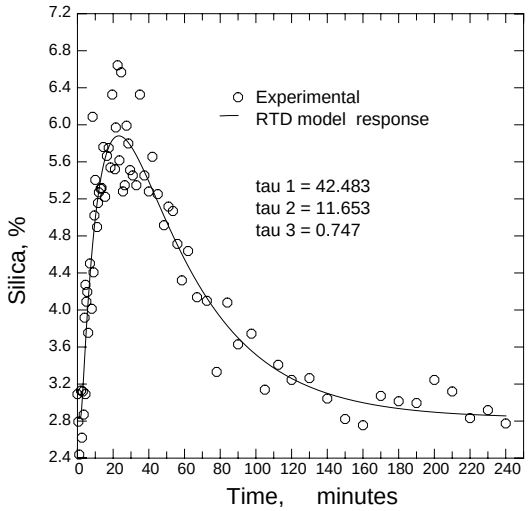

Figure 8.15 Residence-time distribution function for solids in a continuously operating ball mill. The line is the small-small-large segment model response to the experimental data.

The residence-time distribution function for a mill can be measured experimentally by means of a dynamic tracer test. It is considerably easier to trace the liquid phase than the solid phase but the two phases have different residence-time distributions. The water is not restricted during its passage through the mill as much as the solid phase is. Consequently the hold-up of solid in the mill is greater than that of the liquid and the solid has a higher mean residence time. Although the two phases have significantly different mean residence times, the behavior of each phase is consistent with the three-stage model that is described above. This is demonstrated in the two measured residence time distributions that are shown in Figures 8.14 and 8.15.

8.4 Models for Rod Mills

The physical arrangement of rods in the rod mill inhibits the effective internal mixing that is characteristic of ball mills. The axial mixing model for the mixing pattern is more appropriate than that based on the perfectly-mixed region. When axial mixing is not too severe in the mill, an assumption of plug flow is appropriate. In that case the population balance model for the batch mill can be used to simulate the behavior of the rod mill with the time replaced by the average residence time in the mill which is equal to the holdup divided by the throughput.

8.5 The Population Balance Model for Autogenous Mills

Four distinct mechanisms of size reduction have been identified in fully autogenous mills: attrition, chipping, impact fracture and self breakage. Attrition is the steady wearing away of comparatively smooth surfaces of lumps due to friction between the surfaces in relative motion. Chipping occurs when asperities are chipped off the surface of a particle by contacts that are not sufficiently vigorous to shatter the particle. Attrition and chipping are essentially surface phenomena and are commonly lumped together and identified as wear processes. Impact fracture occurs when smaller particles are nipped between two large particles during an impact induced by collision or rolling motion. Self breakage occurs when a single particle shatters on impact after falling freely in the mill. Rates of breakage and the progeny spectrum formed during these processes differ considerably from each other and each should be modeled separately.

A fifth breakage mechanism occurs in a semi-autogenous mill when particles are impacted by a steel ball. Breakage and selection functions that describe this mechanism can be modeled in a manner similar to those used for the ball mill.

In practice three distinct fracture sub-processes are modeled: wear, impact fracture, and self breakage. Each of these produces essentially different progeny size distributions and the appropriate breakage function must be used for each. The breakage function for attrition and chipping $A(x;y)$ can be measured in the laboratory in mills that contain only large lumps that are abraded under conditions similar to those found in operating mills. No general models for the attrition breakage function have been developed. The breakage function $B(x;y)$ for the impact fracture process can be modeled using the same model structures that were used for ball milling. The breakage function for self breakage $C(x;y)$ can be modeled using the t_{10} method that describes single-particle impact fracture using the impact energy equal to the kinetic energy of the particle immediately before impact. Particles will have a wide distribution of free-fall impact energies in a real mill and the breakage function for self-breakage is obtained by integration over the impact energy spectrum

$$C(x;y) = \int_0^\infty C(x;y,h)\,P(y,h)p(h)\,dh \tag{8.42}$$

where $C(x;y,h)$ is the single particle breakage function for self-breakage of a particle of size y in free fall from height h, $P(y,h)$ is the probability that a particle of size y will shatter when falling a vertical height h and $p(h)$ is the distribution density for effective drop heights in the mill.

References:

Stanley, G. G. Mechanisms in the autogenous mill and their mathematical representation. S. Afr. Inst Mining Metall. 75(1974)77-98

Leung, K., Morrison R. D. and Whiten W.J. An energy based ore-specific model for autogenous and semi-autogenous grinding. Coper '87 Universidadde Chile (1987-1988) pp 71-85

Goldman, M and Barbery, G. Wear and chipping of coarse particles in autogenous grinding: experimental investigation and modeling. Minerals Engineering 1(1988) pp67-76
Goldman, M, Barbery G. and Flament F. Modelling load and product distribution in autogenous and semi-autogenous mills: pilot plant tests. CIM Bulletin 8 (Feb1991) pp 80-86.

The attrition and wear processes that occur in autogenous, semi-autogenous, and pebble mills produce a significant fraction of the final production of fine particles in the mill. These processes are not satisfactorily described by the kinetic breakage models that are useful for ball and rod mills. It is necessary to invoke the full generalized population balance model that was developed in section 2.13 in order to describe the autogenous milling operations adequately.

Various finite difference representations of equation (2.111) are available but those based on the predefined size classes as described in section 2 are generally used. It is usual and useful to interpret the rate of breakage process R in such a way that

$$\int_{D_i}^{D_{i-1}} R'(p(x),x,F[p(x)])dx \;=\; \bar{R}(p_i,x_i,F[p(x)]) \tag{8.43}$$

is the rate of breakage out of the interval i. This convention, which was used to develop the simple finite difference models for ball and rod mills, is useful particularly because it is comparatively easy to measure the rate of breakage out of a screen interval in the laboratory and to correlate the measured rates with the representative size for a size class.

Equation (2.111) is integrated over a typical size class i to give

$$\begin{aligned} &-\tau\Delta_i\kappa p(x) \;+\; 3\tau\int_{D_i}^{D_{i-1}}\kappa(x)\frac{p(x)}{x}dx \;+\; \tau\bar{R}(p_i,x_i,F_1[p(x)]) \\ &-\;\tau\sum_{j=1}^{i-1}\bar{R}(p_j,x_j,F_1[p(x)])\,\Delta_i B(x,D_j) \;-\; 3\tau\int_{D_i}^{D_{i-1}}\int_{R''(x)}\kappa(x')\frac{p(x')}{x'}a(x;x')\,dx'\,dx \\ &=\; p_{i\,in} \;-\; p_{i\,out} \end{aligned} \tag{8.44}$$

where

$$\Delta_i\kappa p(x) \;=\; \kappa(D_{i-1})p(D_{i-1}) \;-\; \kappa(D_i)p(D_i) \tag{8.45}$$

and

$$\begin{aligned} \Delta_i B(x;D_j) \;&=\; B(D_{i-1};D_j) \;-\; B(D_i,D_j) \\ &=\; \Delta B_{ij} \end{aligned} \tag{8.46}$$

Finite difference approximations are required for the remaining terms in equation (8.44) in terms of the representative size for each size class. The following approximations have been used successfully

$$p(D_i) \;\simeq\; \frac{p_i}{D_i - D_{i+1}} \tag{8.47}$$

so that

$$\Delta_i \kappa p(x) \simeq \frac{\kappa_{i-1} p_{i-1}}{D_{i-1} - D_i} - \frac{\kappa_i p_i}{D_i - D_{i+1}} \tag{8.48}$$

$$\int_{D_i}^{D_{i-1}} \kappa(x) \frac{p(x)}{x} dx \simeq \frac{\kappa_i p_i}{d_{pi}} \tag{8.49}$$

$$\int_{D_j}^{D_{j-1}} \kappa \frac{p(x')}{x'} \int_{D_i}^{D_{i-1}} a(x;x')\, dx\, dx' = \frac{\kappa_j p_j}{d_{pj}} \Delta A_{ij} \tag{8.50}$$

which implies that the products of wear and attrition must leave the size class of the parent particle i.e., must be smaller than D_j.

$$\Delta A_{ij} = A(D_{i-1};D_j) - A(D_i;D_j) \tag{8.51}$$

If the total region is perfectly mixed then $p_i = p_{i\,out}$ and equation (8.44) becomes

$$\begin{aligned} & p_i - \frac{\tau\kappa_{i-1} p_{i-1}}{D_{i-1} - D_i} + \frac{\tau\kappa_i p_i}{D_i - D_{i+1}} + \frac{3\tau\kappa_i p_i}{d_{pi}} + k_i p_i \tau \\ & - \tau \sum_{j=1}^{i-1} \left(k_j \Delta B_{ij} + \frac{3\kappa_j \Delta A_{ij}}{d_{pj}} \right) p_j = p_{i\,in} \end{aligned} \tag{8.52}$$

This equation can be simplified somewhat by defining the ratio

$$\gamma_i = \frac{3\kappa_i}{d_{pi}} \tag{8.53}$$

and

$$\sigma_i = \frac{d_{pi}}{3(D_i - D_{i+1})} \tag{8.54}$$

$$\begin{aligned} & p_i + \sigma_i \gamma_i \tau p_i + \gamma_i \tau p_i \\ & = p_{i\,in} + \sigma_{i-1} \gamma_{i-1} \tau p_{i-1} + \tau \sum_{j=1}^{i-1} \left(k_j \Delta B_{ij} + \gamma_j \Delta A_{ij} \right) p_j \end{aligned} \tag{8.55}$$

$$p_i = \frac{p_{i\,in} + \sigma_{i-1} \gamma_{i-1} \tau p_{i-1} + \tau \sum_{j=1}^{i-1} \left(k_j \Delta B_{ij} + \gamma_j \Delta A_{ij} \right) k_j p_j}{1 + (\sigma_i \gamma_i + \gamma_i + k_i) \tau} \tag{8.56}$$

This equation for the well-mixed autogenous and semi-autogenous mill was first derived by Hoyer and Austin (D I Hoyer and L G Austin. "A Simulation Model for Autogenous Pebble Mills" Preprint number 85-430 SME-AIME Fall Meeting, Albuquerque Oct 1985).

This equation can be simplified further by making the following definitions

$$\zeta_i = \sigma_i \gamma_i \tau \tag{8.57}$$

$$\xi_i = (k_i + \gamma_i)\tau \tag{8.58}$$

Both ζ_N and ξ_N are zero because there is no breakage out of the smallest size class.

$$(k_j \Delta B_{ij} + \gamma_j \Delta A_{ij})\tau = \Delta_{ij} \tag{8.59}$$

Using the definitions of ΔA_{ij} and ΔB_{ij}

$$\sum_{i=j+1}^{N} \Delta_{ij} = (k_j + \gamma_j)\tau = \xi_j \tag{8.60}$$

Equation (8.56) can be written

$$p_i = \frac{p_{iin} + \zeta_{i-1} p_{i-1} + \sum_{j=1}^{i-1} \Delta_{ij} p_j}{\zeta_i + \xi_i + 1} \tag{8.61}$$

This is the fundamental discrete population balance equation for autogenous mills. The appearance of the term p_{i-1} on the right hand side of equation (8.61) should be particularly noted. This term arises from the wear process that reduces the size of large lumps in the mill charge which is an essential feature of autogenous milling. Equation (8.61) can be solved recursively in a straightforward manner starting at p_0. However it is necessary to choose a value of $\zeta_0 p_0$ to ensure that the discrete analogue of (2.86)

$$\sum_{i=1}^{N} p_i = 1 \tag{8.62}$$

is satisfied.
Using equation (8.61)

$$\begin{aligned}\sum_{i=1}^{N} p_i(1+\xi_i+\zeta_i) &= \sum_{i=1}^{N} p_{iin} + \sum_{i=1}^{N} \zeta_{i-1}p_{i-1} + \sum_{i=1}^{N}\sum_{j=1}^{i-1} \Delta_{ij}p_j \\ &= 1 + \zeta_0 p_0 + \sum_{i=2}^{N} \zeta_{i-1}p_{i-1} + \sum_{j=1}^{N-1} p_j \sum_{i=j+1}^{N} \Delta_{ij} \\ &= 1 + \zeta_0 p_0 + \sum_{j=1}^{N-1} \zeta_j p_j + \sum_{j=1}^{N-1} p_j \xi_j \\ &= 1 + \zeta_0 p_0 + \sum_{j=1}^{N-1} (\zeta_j+\xi_j)p_j\end{aligned} \tag{8.63}$$

which leads to

$$\sum_{i=1}^{N} p_i + (\zeta_N+\xi_N)p_N = 1 + \zeta_0 p_0 \tag{8.64}$$

Thus the condition

$$\zeta_0 p_0 = 0 \tag{8.65}$$

guarantees the consistency of the solution.

8.5.1 The effect of the discharge grate

In practice it is always necessary to maintain some classification action at the mill discharge to ensure that large pebbles do not escape from the mill. Autogenous and semi-autogenous mills are always equipped with a steel or rubber grate to hold back the grinding media. The classification action of the grate can be described in terms of a classification function c_i as was done in Section 8.2.2. Application of equation (8.61) to the mill contents gives

$$m_i = \frac{f_i' + \zeta_{i-1}m_{i-1} + \sum_{j=1}^{i-1} \Delta_{ij}m_j}{1 + \zeta_i + \xi_i} \tag{8.66}$$

where

$$f_i' = \frac{p_i^F}{1+C} + c_i m_i \tag{8.67}$$

and C is the fraction of the total stream that is returned to the mill by the classification action at the discharge end. The residence time to be used to calculate ζ_i, ξ_i, and Δ_{ij} in equation (8.66) is

$$\tau' = \frac{M}{(1+C)W} = \frac{\tau}{1+C} \tag{8.68}$$

$$m_i = \frac{\frac{p_i^F}{1+C} + \zeta_{i-1} m_{i-1} + \sum_{j=1}^{i-1} \Delta_{ij} m_j}{1 + \zeta_i + \xi_i - c_i} \tag{8.69}$$

Define a new variable

$$m_i^* = (1+C) m_i \tag{8.70}$$

and this equation becomes

$$m_i^* = \frac{p_i^F + \zeta_{i-1} m_{i-1}^* + \sum_{j=1}^{i-1} \Delta_{ij} m_j^*}{1 + \zeta_i + \xi_i - c_i} \tag{8.71}$$

which can be solved recursively starting from i = 1and $\zeta_0 m_0^* = 0$. The value of τ' must be established by iterative calculation using equation (8.68) after C is recovered from

$$C = \sum_{i=1}^{N} c_i (1+C) m_i = \sum_{i=1}^{N} c_i m_i^* \tag{8.72}$$

The iterative calculation starts from an assumed value of τ' and is continued until the value of τ' stabilizes. The size distribution from the mill is recovered from

$$p_i = (1-c_i) m_i^* \tag{8.73}$$

The kinetic parameters k_i and κ_i and the breakage functions $A(D_i; D_j)$ and $B(D_i, D_j)$ must be estimated* from experimental data.

8.6 Models for the Specific Rate of Breakage in ball mills

The utility the kinetic model for breakage depends on the availability of robust models for the specific rate of breakage to describe specific milling conditions. Both functions are strong functions of the milling environment. Factors which affect the rate of breakage are the mill diameter, mill speed, media load and size and particle hold-up.

The most important functional dependence is between the specific rate of breakage and the particle size and methods for the description of this functional dependence are described below. The specific rate of breakage increases steadily with particle size which reflects the decreasing strength of the particles as size increases. This is attributed to the greater density of microflaws in the interior of larger particles and to the greater likelihood that a particular large particle will contain a flaw that will initiate fracture under the prevailing stress conditions in a mill. The decrease in particle strength does not does not lead to an indefinite increase in the specific rate of breakage. As the particle size becomes significant by comparison to the size of the smallest media particles, the prevailing stress levels in the mill are insufficient to cause fracture and the specific rate of breakage passes through a maximum and decreases with further increase in particle size. Some typical data are shown in Figure 8.16.

8.6.1 The Austin model for the specific rate of breakage.

Austin represents the variation of the specific rate of breakage with particle size by the function

$$k(d_p) = \frac{k_0 d_p^{\alpha}}{1 + \left(d_p/\mu\right)^{\Lambda}} \tag{8.74}$$

and it is usual to specify the particle size in mm and the specific rate of breakage in min^{-1}.

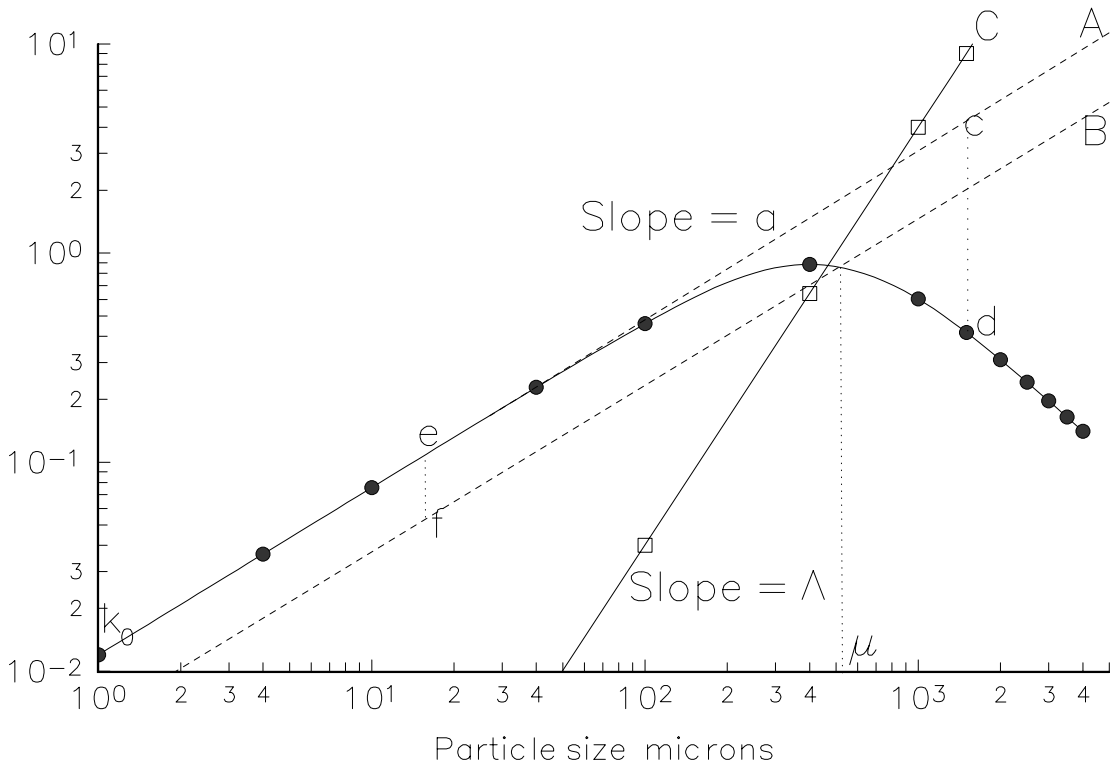

Figure 8.16 Graphical procedure for the determination of the parameters in Austin's selection function.

It is useful to relate the individual parameters in this function to specific features of the graph of $k(d_p)$ plotted against d_p. A typical plot of this function is shown in Figure (8.16) and it has a maximum at a particle size somewhat smaller than the parameter μ which essentially fixes the position of the maximum. The maximum occurs in the specific rate of breakage because as the particles get larger they are less likely to be broken during any typical impact in the mill. The specific particle fracture energy decreases as size increases according to equation (8.10) but the rate of decrease reduces as the particle size increases and eventually becomes approximately constant for particles larger than a few millimeters for most ores. Consequently the particle fracture energy increases at a rate approximately proportional to the particle mass. Thus for a given impact energy larger particles have a smaller probability of breaking since the energy that a particle absorbs from the impact must exceed its fracture energy otherwise it will not break.

The graphical procedure is implemented as follows:

i) Extend the initial straight line portion of the data curve as straight line *A* having equation

$$k = k_0 d_p^{\alpha} \tag{8.75}$$

ii) k_0 is evaluated at the intersection of the straight line with the ordinate d_p = 1 mm. α is equal to the slope of the line. K_0 is often represented by the symbol S_1 which is called the selection function at 1 mm.

iii) Evaluate ratios such as *c/d* to form $\frac{k_0 d_p^{\alpha}}{k(d_p)}$ at a number of particle sizes as shown.

Plot $\frac{k_0 d_p^{\alpha}}{k(d_p)} - 1$ against the particle size as shown as line *C* in Figure (8.74). The slope of the resulting line is equal to Λ because, according to equation (8.74),

$$\frac{k_0 d_p^{a}}{k(d_p)} - 1 = \left(d_p/\mu\right)^{\Lambda} \tag{8.76}$$

Parameter μ can be evaluated in one of two ways.
Construct line *B*, parallel to line *A* and passing through a point *f* which has ordinates equal to *0.5e*.
This line intersects the data curve at abscissa value μ as shown.
Alternatively the size at which $k(d_p)$ is a maximum is given by

$$\frac{dk_0(d_p)}{d\,d_p} = 0 \tag{8.77}$$

which implies that

$$d_{p\max} = \left(\frac{\Lambda}{\alpha} - 1\right)^{-\frac{1}{\Lambda}} \tag{8.78}$$

8.6.2 Scale-up of the Austin selection function

When developing scale-up rules for the specific rate of breakage, it is necessary to distinguish between parameters that are material specific and those that depend on the material that is to be milled and also on the geometrical scale of the mill that is to be used. The parameters α and Λ in the Austin model for specific rate of breakage are usually assumed to be material specific only while k_0 and μ depend on the geometrical scale.
The graphical construction that is outlined in the previous section reveals the role that each parameter in the Austin selection function plays in determining the specific rate of breakage in a ball mill. It is not difficult to determine the values of these parameters from data obtained in a batch milling experiment in the laboratory. They can also be

estimated using standard parameter estimation techniques from the size distributions in samples taken from the feed and discharge streams of an operating mill.

In order to use this model for simulation of other mills it is necessary to use scale-up laws that describe how these parameters vary with variations of the mill size and the environment inside the mill. The dominant variables are the mill diameter D_m and the size of the balls that make up the media d_b. These variables together determine the average impact energy in the mill and both have a significant influence on the value of the constant k_0 in equation (8.74). Because the specific rate of breakage is essentially a kinetic parameter, it obviously increases with the number of impacts that occur per second per unit volume in the mill. Geometrically similar mills having the same fractional filling by media and rotating at the same fraction of critical speed φ_c will produce nearly identical impact frequencies per unit volume. The impact frequency per unit volume should vary at a rate proportional to the speed of rotation. The variation of impact frequency with mill filling is rather more complex and purely empirical scale-up rules must be applied. The effect of interstitial filling is also modeled empirically to reflect the fact that not all of the slurry remains in the region of the tumbling media where energetic impacts occur. A pool of slurry can accumulate at the toe of the charge for example and this is largely devoid of impact that cause breakage. As the interstitial fill fraction approaches 1.0 the impacts are increasingly cushioned by excess slurry between media particles. The scale-up law for parameter k_0 is

$$\frac{k_0}{k_{0T}} = \left(\frac{D_m}{D_{mT}}\right)^{N_1}\left(\frac{1 + 6.6J_T^{2.3}}{1 + 6.6J^{2.3}}\right)\left(\frac{\varphi_c - 0.1}{\varphi_{cT} - 0.1}\right)\left(\frac{1 + \exp[15.7(\varphi_{cT} - 0.94)]}{1 + \exp[15.7(\varphi_c - 0.94)]}\right)\exp[-c(U - U_T)] \qquad (8.79)$$

The subscript T in this equation refers to the variable determined under the test conditions for which the parameters are estimated and the corresponding variable without this subscript refers to the large scale mill that must be simulated. The variables J and U are define by the load when the mill is stationary as shown in Figure 8.17.

The media ball size also influences the specific rate of breakage. Smaller ball sizes produce less energetic impacts and each impact influences fewer particles in the immediate vicinity of the impact point between any two balls. The active zone in the slurry between balls is obviously smaller with smaller balls. Smaller balls are also less efficient at nipping larger particles. Offsetting these effects that tend to decrease the specific rate of breakage as ball size decreases is the increased frequency of impact that results from the increased number of smaller balls in the mill. The number of balls per unit volume varies as $1/d^3$. The net result of these competing effects is revealed by experiment which show that the specific rate of breakage scales as $1/d^n$ where n is approximately equal to 1while the particle size at maximum specific rate of breakage increases in direct proportion to the ball size. The parameter μ which defines the size at which the specific rate of breakage is a maximum increases with ball size raised to a power close to 1 and also shows a power dependence on the mill diameter. Operating mills always contain a distribution of ball sizes and to accommodate this the scale-up is weighted in proportion to the mass of balls in each size.

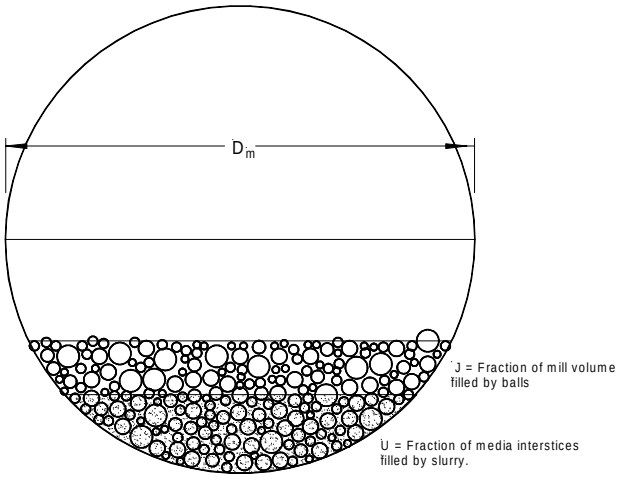

Figure 8.17 The geometrical constants for mill scale-up are defined by the load conditions when the mill is stationary.

$$k(d_p) = k_0 d_p^{\alpha} \sum_k \frac{m_k \left(\frac{d_T}{d_k} \right)^{N_0}}{1 + \left(\frac{d_p}{\mu_k} \right)^{\Lambda}} \tag{8.80}$$

where d_k is the representative diameter of the kth ball size class and m_k is the mass fraction of the ball size class in the mill charge. μ_k is given by

$$\frac{\mu_k}{\mu_{kT}} = \left(\frac{D_m}{D_{mT}} \right)^{N_2} \left(\frac{d_k}{d_T} \right)^{N_3} \tag{8.81}$$

Recommended values for the constants are $N_0 = 1.0$, $N_1 = 0.5$, $N_2 = 0.2$, $N_3 = 1.0$ and $c = 1.3$. Large size ball mills have been observed to operate inefficiently so that k_0 should be scaled by the factor $(3.81/D_m)^{0.2}$ when the diameter of this type of mill exceeds 3.81 meters.

Austin LG Menacho JM and Pearchy F A general model for semi-autogenous and autogenous milling. APCOM87. Proc 20th Intnl Symp on the Application of Computers and Mathematics in the Mineral Industries. Vol 2 SAIMM 1987 pp 107 - 126

8.6.3 The Herbst-Fuerstenau model for the specific rate of breakage.

The variation of the specific rate of breakage and of the breakage function with milling conditions can be substantially accounted for by describing the variation of these functions with the specific power input into the mill and examining how the specific power input varies with mill size and with design and operating conditions. This indirect method is particularly useful for scaling up the functions from batch scale and pilot scale testwork. This is called the energy-specific scale-up procedure and was developed initially by Herbst and Fuerstenau. (Int Jnl Mineral Processing 7 (1980) 1-31)

The specific rate of breakage out of size class i is proportional to the net specific power input to the mill charge.

$$k_i = S_i^E \frac{P}{M} \tag{8.82}$$

where P is the net power drawn by the mill exclusive of the no-load power that is required to overcome mechanical and frictional losses in the mill. M is the mass of the charge in the mill excluding the media. S_i^E is called the energy-specific selection function for particles in size class i. The energy-specific breakage rate is commonly reported in tonnes/kWhr. The essential feature of the Herbst-Fuerstenau model is that S_i^E is a function of the material only and does not vary with milling conditions nor with mill size. This assumption is equivalent to the postulate that the amount of breakage that occurs inside the mill is proportional to the amount of energy that has been absorbed by the material that is being milled and it is immaterial how the energy is actually imparted to the particles or at what rate. Thus the method can be used to scale up the breakage rates over broad operating ranges. In fact it has been found from experimental observations that S_i^E is a function of the ball media size distribution in the mill. It should be determined in a laboratory experiment using the same ball size distribution as the full-scale mill that is to be modeled or simulated.

It is usually convenient to use equation (8.82) in the form

$$k_i\tau = S_i^{E}\frac{P}{W} \tag{8.83}$$

where W is the mass flowrate of solids through the mill. The product $k\tau$ can be used in equations (8.32), (8.38) and (8.61) and neither the mean residence time τ of the solids in the mill nor the specific rate of breakage k_i need be known explicitly. This eliminates the need for complex empirical scale-up rules such as equation 8.79. The ratio P/W, which is measured in kWhr/tonne is the net specific power consumption in the mill.

The variation of energy-specific breakage rate with particle size is given by

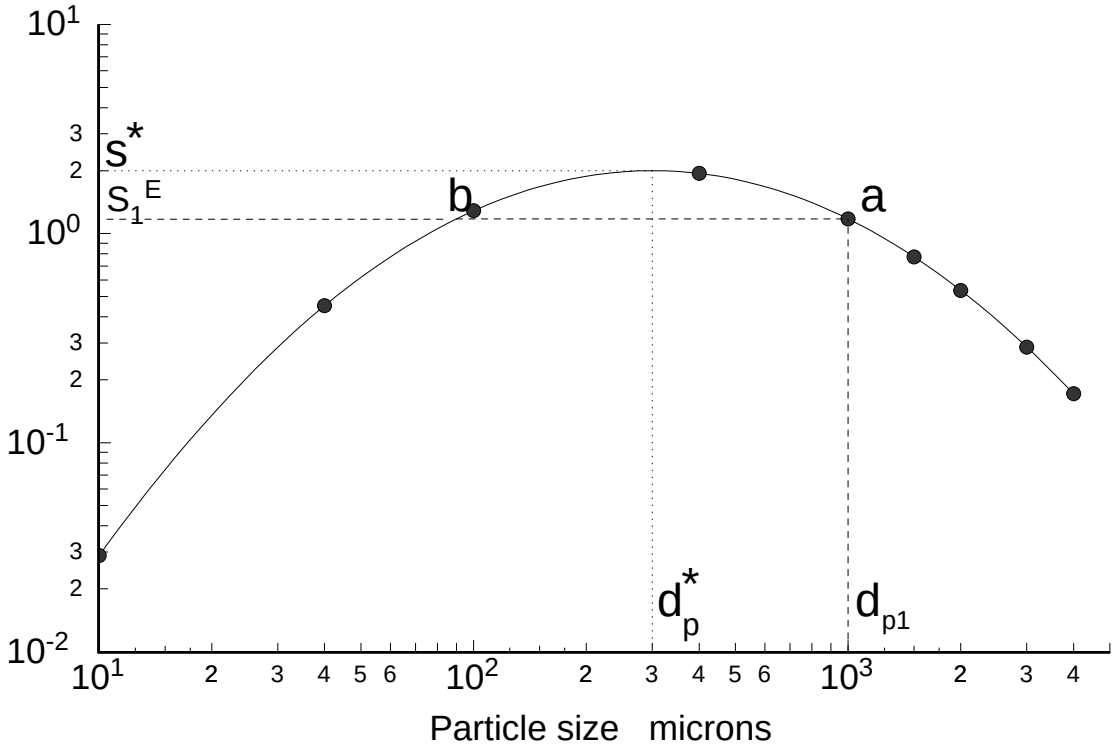

Figure 8.18 Graphical procedure for the determination of the parameters in the Herbst-Fuerstenau energy-specific rate of breakage.

$$\ln\left(S_i^E/S_1^E\right) = \zeta_1\ln\left(d_{pi}/d_{p1}\right) + \zeta_2\left[\ln\left(d_{pi}/d_{p1}\right)\right]^2 + \ldots \tag{8.84}$$

which represents the logarithm of the energy-specific breakage rate as a power series of the logarithm of the particle size. Usually two terms in the series are sufficient to describe the variation in sufficient detail for most purposes so that the function becomes

$$\ln\left(S_i^E/S_1^E\right) = \zeta_1\ln\left(d_{pi}/d_{p1}\right) + \zeta_2\left[\ln\left(d_{pi}/d_{p1}\right)\right]^2 \tag{8.85}$$

A typical plot of this function is shown in Figure (8.19).

The parameters in this functional form can be obtained from experimental data using the following simple graphical procedure.

i) A suitable reference size d_{p1} is chosen to give the reference value S_1^E at point *a* on the curve. d_{p1} is usually taken as the top size for the problem on hand but that is not essential.

ii) The turning point on the curve is located midway between points *a* and *b* and the coordinates of the turning point are (d_p^*, S^*).

iii) The parameters in the selection function are related to the coordinates of the turning point by

$$\zeta_1 = \frac{2\ln\left(S^*/S_1^E\right)}{\ln\left(d_p^*/d_{p1}\right)} \tag{8.86}$$

and

$$\zeta_2 = -\frac{\ln\left(S^*/S_1^E\right)}{\left[\ln\left(d_p^*/d_{p1}\right)\right]^2} \tag{8.87}$$

These expressions are obtained by differentiating equation (8.85) and setting the result to zero.

$$0 = \zeta_1 + 2\zeta_2\ln\left(d_p^*/d_{p1}\right) \tag{8.88}$$

This must be solved simultaneously with

$$\ln\left(S^*/S_1^E\right) = \zeta_1\ln\left(d_p^*/d_{p1}\right) + \zeta_2\left[\ln\left(d_p^*/d_{p1}\right)\right]^2 \tag{8.89}$$

which yields equations (8.86) and (8.87).

This model for the variation of specific rate of breakage with particle size is useful to model the effect of ball size distribution in the mill. The parameter ζ_2 determines the sharpness of the maximum in the plot of S_i^E against the particle size as shown in Figure 8.18. ζ_2 must always be a negative number otherwise the graph will have a minimum rather than a maximum. Large numerical values of ζ_2 make the peak in the curve sharper and consequently the rate of breakage falls off rapidly at the smaller particle sizes. Conversely smaller values of ζ_2 make the peak flatter and breakage rates are

maintained even at comparatively small sizes. Smaller media are associated with smaller values of ζ_2. ζ_1 determines the particle size at maximum specific breakage rate through the expression

$$\ln\left(\frac{d_p^*}{d_{p1}}\right) = -\frac{\zeta_1}{2\zeta_2} \tag{8.90}$$

The use of the energy-specific selection function to scale up ball mill operations is described in the following papers.
Herbst JA, Lo YC, and Rajamani K, Population balance model Predictions of the Performance of Large-Diameter Mills. *Minerals and Metallurgical Engineering, May 1986, pp114-120*
Lo YC, and Herbst JA, Cosideration of Ball Size Effects in the Population Balance Approach to Mill Scale-Up. In Advances in Mineral Processing. P Somasudaran Ed. Society of Mining Engineers Inc. Littleton, 1986 pp33-47.
Lo Yc and Herbst JA., Analysis of the Performance of Large-Diameter Mills at Bougainville using the population balance approach. *Minerals and Metallurgical Processing*, Nov 1988 pp221-226.

8.6.4 Specific rate of breakage from the impact energy spectrum.

The selection function can be calculated from the fundamental breakage characteristics of the particles. The selection function is essentially a measure of the likelihood that a particle will be broken during a specific impact event. In order for a particle to be "selected for breakage" during the event it must be involved with the event (ie it must be in the impact zone between two media particles) and it must receive a sufficiently large fraction of the event impact energy so that its fracture energy is exceeded. Integrating over all the impacts in the mill gives

$$\text{Specific rate of breakage} = \int_0^{\infty} p(E)\, w(d_p,E) \int_0^1 P(E,d_p)\, p(e)\, de\, dE \tag{8.91}$$

The following assumptions were used for each of the terms in equation (8.91).
Partition of energy among particles involved in the impact

$$p(e) = \frac{0.3726}{(e-0.1)^{1.1}} \tag{8.92}$$

Mass involved in the impact from single impact measurements on beds of particles.

$$w(d_p,E) = k d_p^{1/2} E^{0.4} \quad \text{kg} \tag{8.93}$$

Distribution of impact energies in the mill based on DEM simulations

$$p(E) = \beta\alpha_1^2 E \exp(-\alpha_1 E) + (1-\beta)\alpha_2 \exp(-\alpha_2 E) \tag{8.94}$$

The probability of breakage $P(E,d_p)$ is log normal with

$$E_{50} = 56\left(1+\frac{1}{d_p}\right)^2 \quad \text{J/kg} \tag{8.95}$$

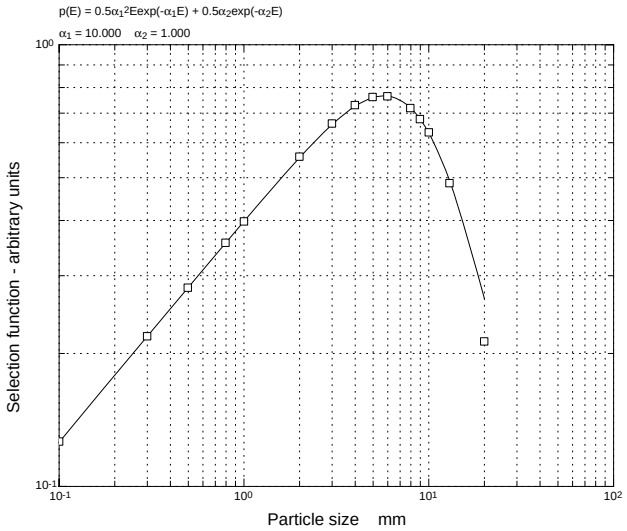

Figure 8.19 Specific rate of breakage calculated from equation (8.91) (plotted points) compared to the Austin function equation (8.96) (solid line).

These expressions were substituted into equation (8.91) and the result is compared with the standard Austin function in Figure (8.20).

$$k = \frac{0.4 d_p^{0.5}}{1 + (d_p/10)^{2.51}} \tag{8.96}$$

8.7 Models for the Specific Rate of Breakage in Autogenous and Semi-Autogenous Mills

The essential features of an autogenous or semi-autogenous mill are shown in Figure 8.20 The most significant difference between ball milling and autogenous milling is the presence of considerably larger particles of ore in the charge. These are added in the mill feed and act as grinding media. Consequently the average density of the media particles is considerably less than in the ball mill and this results in lower values for the specific rate of breakage when compared to ball or rod mills. The average density of the load is proportionately less also and as a result autogenous mills can be built with significantly larger diameters.

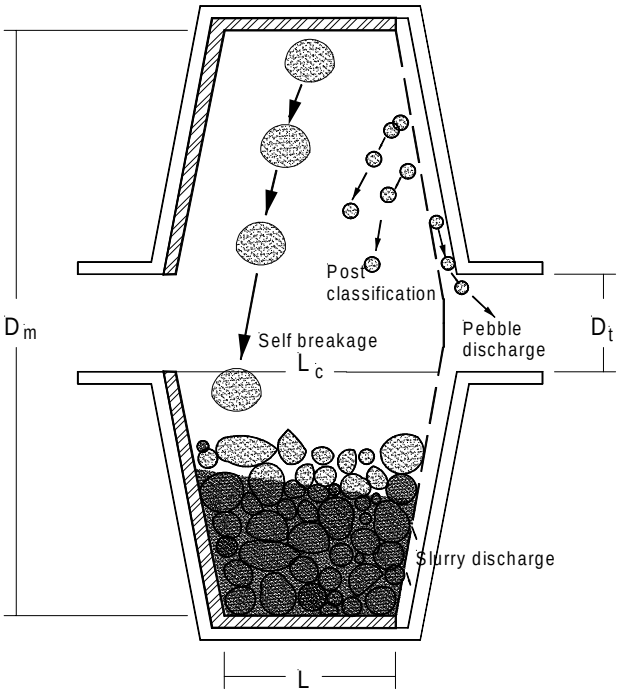

Figure 8.20 Schematic sketch of autogenous mill.

Equations (8.71) define the size distribution in the charge of an autogenous or semi-autogenous mill using the population balance model. The size distribution in the mill discharge can be calculated from the size distribution of the charge using equation (8.73). In order to use these equations it is necessary to be able to calculate the selection functions and breakage functions for the separate breakage mechanisms that occur in the mill namely attrition, chipping impact fracture and self breakage. Chipping and attrition occur on the surface of the particle and the inner core of the particle is not affected. Particles are subject to attrition through friction between particles and also between particles and the walls of the mill. Particles are chipped through impact against other particles or against the walls of the mills. The size distribution of the progeny from attrition is somewhat finer than that from chipping but these two subprocesses are normally lumped together. Goldman et. al. (1988, 1991) and Austin et. al (1987, 198) have measured wear rates in comparatively small test mills in batch mode and all the data can be described by a wear model of the type

$$\kappa_i = \kappa d_{pi}^{\Delta} \tag{8.97}$$

Austin et. al. favor $\Delta = 0$ while Goldman et. al. (1991) found $\Delta = 0.37$ in a 1.75 m diameter pilot plant mill and $\Delta = 1$ in a 0.75 m laboratory mill (Goldman et. al. 1988). The surface specific wear rate depends on the milling environment decreasing as the proportion of fines increases in the mill charge and increasing with mill load and mill diameter. Careful experiments have shown that the surface specific wear rate on a particular particle decreases for several minutes after it has been introduced into the mill environment because its initial rough surface is subject to chipping and attrition that decreases as the particle becomes rounded. Because of this phenomenon the population balance equation should also allow for a distribution of sojourn times of the particles in the mill. This level of fine detail is not justified at the level of modeling that is described here.

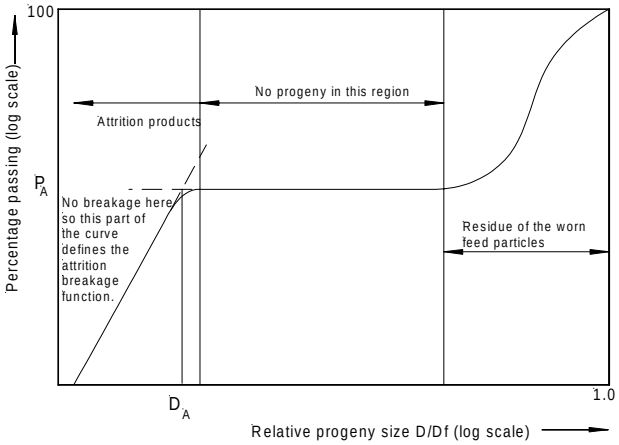

Figure 8.21 Schematic of a typical progeny size distribution from a 10 minute tumbling test.

The value of the specific attrition rate κ is ore specific and should be measured experimentally for the ore. An attrition method has been developed at Julius Kruttschnitt Mineral Research Center and is described in their 25th anniversary volume. A sample of the material in the 38 mm to 50 mm size range is tumbled for 10 minutes. The size distribution of the charge after this time is determined by screening as is typically bimodal as shown in Figure 8.21.Estimates of the specific attrition rate and the attrition breakage function can be easily estimated from this graph. From equation (2.104)

$$\frac{dm}{dt} = -\kappa\frac{\pi\rho_s x^{2+\Delta}}{2} = -\kappa\frac{3m}{x^{1-\Delta}} \tag{8.98}$$

Since the particles do not change much in size during the test, x and m can be assumed constant .

$$\frac{dm}{dt} = -3\kappa\frac{m(0)}{d_f^{1-\Delta}} \tag{8.99}$$

where d_f is the geometric mean size of the original feed particles and simple integration gives

$$m(t) - m(0) = -3\kappa\frac{m(0)}{d_f^{1-\Delta}} \tag{8.100}$$

and

$$\frac{P_A}{100} = \frac{m(0) - m(t)}{m(0)} = \frac{3\kappa\Delta t}{d_f^{1-\Delta}} \tag{8.101}$$

Since the plateau in Figure 8.21 Usually includes the point $D/D_f = 0.1$, P_A is closely related to the t_a parameter that is quoted in the JKMRC attrition test result. The fraction of the original particles that has degraded by attrition during the test is equal to P_A, the height of the plateau on the cumulative size distribution curve. Thus

$$P_A = 10t_A$$
$$\kappa = \frac{d_f^{1-\Delta}P_A}{300\Delta t} = \frac{d_p^{1-\Delta}t_A}{300\times 60} \qquad \mathrm{m}^{1-\Delta} \tag{8.102}$$

The specific rate of breakage due to impact follows the pattern observed in ball mills and the Austin method can be used to model the specific rate of breakage due to impact fracture provided that due allowance is made for the lower density of the medium particles. In semi-autogenous mills due allowance must be made for the presence of steel balls as well as autogenous media. These effects are modeled by the Austin scale-up procedure by including the autogenous media in the media size classes in equation (8.79). However the lower density of the media particles must be allowed for and in equation (8.80) both m_k and μ_k must be scaled by the ratio ρ_k/ρ_s where ρ_k is the density of media particles in media size class k and ρ_s is the density of the balls in the test mill.

The sharp decrease in the specific rate of breakage that is evident for particles that are too large to be properly nipped during an impact event is especially important in autogenous and semi-autogenous mills because the coarse feed supplies many particles in this size range. An intermediate size range exists in the autogenous mill in which the particles are too large to suffer impact breakage but are too small to suffer self breakage. Particles in this size range can accumulate in the mill because they neither break nor are they discharged unless appropriate ports are provided in the discharge grate. This is the phenomenon of critical size build up.

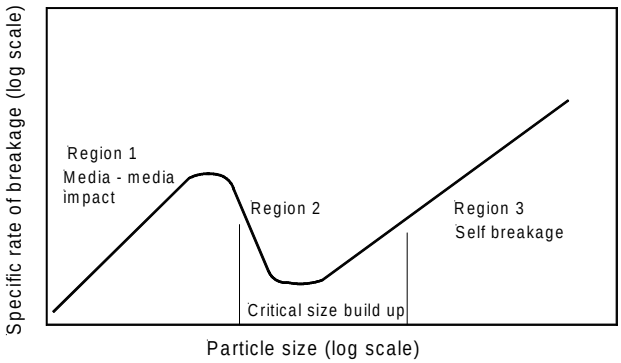

Figure 8.22 Schematic representation of the specific rate of breakage in SAG an FAG mills.

The phenomenon of self breakage is completely absent in ball mills but it plays an important role in autogenous milling. The larger the particle and the greater its height of fall in the mill, the larger its probability of self breakage on impact. Particles smaller than 10 mm or so have negligible breakage probabilities and consequently very low values of the specific rate of self breakage. Specific rates of breakage by impact fracture and self breakage are additive and the variation of k_i with particle size over the entire size range is shown schematically in Figure 8.22. The overall model is obtained from equations 8.74 and 5.8.

$$k_i = \frac{k_0 d_p^{\alpha}}{1 + \left(d_p/\mu\right)^{\Lambda}} + \text{drop frequency}\times G\left[\frac{\ln\left(E/E_{50}\right)}{\sigma_E}\right] \tag{8.103}$$

In equation (8.103) E is the average kinetic energy per unit mass of a lump of size d_p when it impacts the liner or the charge after being released at the top of the mill during tumbling. This is calculated as the potential energy of the particle at a fraction of the inside diameter of the mill. E_{50} is the median particle fracture energy of a lump of size d_p. For larger lumps this is independent of size as given by equation (5.10) but is material specific. The drop frequency is calculated from the asumption that each lump will be dropped once per revolution of the mill.

$$E = fgD_m \qquad \text{J} \tag{8.104}$$

and drop frequency = $0.705 \times \varphi_c / D_m^{½}$ from equation (5.50).

8.8 Models for the Breakage Functions in Autogenous and Semi-Autogenous Mills

The breakage function for impact and self breakage is determined primarily by the impact energy level and the t_{10} method is used as the model as described in Section 5.4.2 For self breakage, the impact energy is a function of the lump size and the height of the drop and this is calculated as the potential energy of the lump at ½ the inside diameter of the mill. For impact breakage the average energy is calculated as the net specific power input to the mill charge.

The breakage function for the products of attrition and chipping can be obtained from the size distribution of the products of the single batch attrition test because there is no significant rebreakage of the attrition products during the test. This breakage function is modeled using a simple logarithmic distribution

$$A(x,D_A) = \left(\frac{x}{D_A} \right)^{\lambda_A} \tag{8.105}$$

D_A is the largest fragment formed by attrition which can be obtained from the measured attrition progeny size distribution as shown in Figure 8.21. λ_A is the slope of the straight line portion of the curve in the attrition product region.

The breakage function for impact fracture is modeled using the same models as for ball mills. The breakage function for self breakage can be determined by dropping individual lumps of ore and determining the size distribution of the products.

8.9 Mill Power and Mill Selection.

8.9.1 The Bond method

The correlation between material toughness and power required in the comminution machine is expressed by the empirical Bond equation. The work done in reducing a mass of material from representative size d_{80}^F to representative size d_{80}^P is given by the Bond equation (5.27)

$$P_o = K\left(\frac{1}{\left(d_{80}^P\right)^{½}} - \frac{1}{\left(d_{80}^F\right)^{½}} \right) \qquad \text{kWhr/ton} \tag{8.106}$$

A reference condition is the hypothetical reduction of 1 ton of material from a very large size to a representative size of 100 microns. This reference energy is called the work index of the material *WI*.

$$WI = K\left(\frac{1}{(100)^{½}} - 0 \right) = \frac{K}{10} \quad \Rightarrow \quad K = 10WI \tag{8.107}$$

$$P_o = 10WI\left(\frac{1}{\left(d_{80}^P\right)^{½}} - \frac{1}{\left(d_{80}^F\right)^{½}} \right) \tag{8.108}$$

in these equations d_{80} must be specified in microns.

The representative size is conventionally taken as the 80% passing size. *WI* can be determined from a standard laboratory test procedure. The Bond equation can be used for crushers, rod and ball mills. *WI* is usually different for these three operations and must be measured separately. The standard laboratory test for the measurement of the Bond work index was designed to produce an index that would correctly predict the power required by a wet overflow discharge ball mill of 2.44 m diameter that operates in closed circuit with a classifier at 250% circulating load. $D_{80}{}^{F}$ and $d_{80}{}^{P}$ in equation (8.108) refer to the feed to the circuit as a whole and the product from the classifier.

The work index for the ore as measured using the standard laboratory method must be adjusted to account for various operating conditions before applying it to calculate the energy requirements of an industrial mill that differ from this standard. This is done by multiplying the measured work index by a series of efficiency factors to account for differences between the actual milling operation and the standard conditions against which the work index was originally calibrated. (Rowland C A Using the Bond work index to measure the operating comminution efficiency. *Minerals & Metallurgical Processing* 15(1998)32-36)

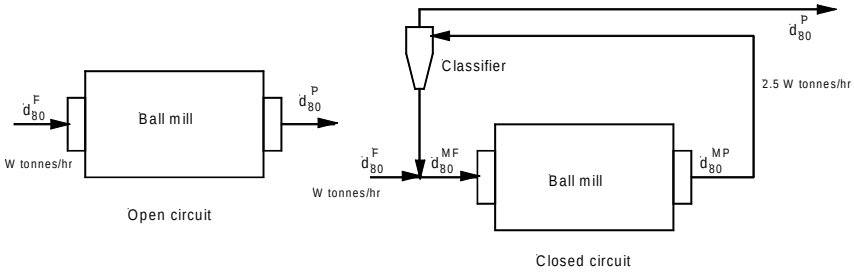

Figure 8.23 Application of Bond work index for calculating power required for open and closed milling circuits

The efficiency factors are:

EF_1: Factor to apply for fine grinding in closed circuit in ball mills = 1.3.

EF_2: Open circuit factor to account for the smaller size reduction that is observed across the mill itself (open circuit condition) as opposed to the size reduction obtained across the closed circuit. If two ball mill circuits, one open and the other closed, as shown in Figure 8.23. If both circuits produce the same $d_{80}{}^{P}$ the power required for the closed circuit is given directly by the Bond formula

$$P_{CC} = 10\mathrm{WI}\left(\frac{1}{(d_{80}^{P})^{½}} - \frac{1}{(d_{80}^{F})^{½}}\right) \qquad (8.109)$$

and the power required by the open circuit is given by

Table 5. Bond work index efficiency factor for wet open circuit milling.

Reference % passing	Open circuit efficiency factor EF_2
50%	1.035
60%	1.05
70%	1.10
80%	1.20
90%	1.40
92%	1.46
95%	1.57
98%	1.70

$$P_{OC} = 10 \times EF_2 \times WI \left(\frac{1}{(d_{80}^{P})^{½}} - \frac{1}{(d_{80}^{F})^{½}} \right) \tag{8.110}$$

with $EF_2 = 1.2$

If the two circuits are required to match their product passing size at a different % passing say $d_{90}{}^{P}$, the factor EF_2 will have the different value as given in Table 5.

EF_3: Factor for variation in mill diameter. Larger mills are assumed to utilize power somewhat more efficiently than smaller mills. This factor is calculated from

$$\begin{aligned} EF_3 &= \left(\frac{2.44}{D_m} \right)^{0.2} && \text{for} \quad D_m < 3.81 \\ &= 0.914 && \text{for} \quad D_m \geq 3.81 \end{aligned} \tag{8.111}$$

EF_4: Oversize feed factor. The optimal $d_{80}{}^{F}$ size for a ball mill that grinds material having a work index of WI kW hr/tonne is given by

$$F_O = 4 \times \left(\frac{14.3}{WI} \right)^{½} \quad \text{mm} \tag{8.112}$$

When the feed has a size distribution coarser than the optimum, the mill must draw more power to achieve the desired product size. The appropriate efficiency factor is given by

$$EF_4 = 1 + \frac{(WI - 7)(d_{80}^{F} - F_O)}{R_r F_O} \tag{8.113}$$

where R_r is the reduction ratio $\dfrac{d_{80}^{F}}{d_{80}^{P}}$

EF_5: The work index in a ball mill increases when the reduction ratio decreases below 3 and the efficiency factor is given by

$$EF_5 = 1 + \frac{0.013}{R_r - 1.35} \tag{8.114}$$

To size a ball mill or rod mill that must process W tons/hr it is necessary to calculate the mill power required from

$$P = P_o \times W \tag{8.115}$$

and find a mill from the manufacturers catalogue that can accept that power. If manufacturers' data is not available, equations (8.12) or (8.14) can be used to select a suitable mill. This will not produce a unique design for the mill because many combinations of D_m and L will satisfy these equations and the aspect ratio of the mill must be chosen to ensure that the mill will provide sufficient residence time or specific power input to produce the required product size distribution as calculated from equation (8.32) or (8.73). It is important to note that the geometry of the mill will

determine the power input not the tonnage through the mill. The power consumed will give a certain amount of size reduction and the output size will be a function of the tonnage. By contrast a crusher will produce a fixed size reduction ratio and the power will vary to match the tonnage subject to the maximum power available from the motor that is installed on the crusher.

8.10 The Batch Mill

8.10.1 Batch grinding of homogeneous solids

The comminution properties of material are often determined in the laboratory by following the size distribution during milling in a batch mill. In such a test, the mill is charged with a given mass of feed material and the mill is operated without continuous discharge and feed.

The size distribution in the charge in a batch mill changes continuously with time. The mass balance must be written for each size class.

For the top size

$$M\frac{dm_1}{dt} = -k_1 M m_1 \tag{8.116}$$

It is usually adequate to assume that k_1 does not vary with time and this equation can be easily integrated to give

$$m_1 = m_1(0)e^{-k_1 t} \tag{8.117}$$

This solution plots as a straight line on log-linear coords.

For the next size down:

$$M\frac{dm_2}{dt} = -k_2 M m_2 + k_1 M m_1 b_{21} \tag{8.118}$$

$$\frac{dm_2}{dt} + k_2 m_2 = k_1 b_{21} m_1 = k_1 b_{21} m_1(0)e^{-k_1 t} \tag{8.119}$$

This is a first order linear differential equation which has a solution of the form:

$$m_2 = Ae^{-k_2 t} + Be^{-k_1 t} \tag{8.120}$$

where A and B are constants that must be determined from the form of the differential equation and from the initial conditions as follows. First the proposed solution is differentiated

$$\frac{dm_2}{dt} = -Ak_2 e^{-k_2 t} - Bk_1 e^{-k_1 t} \tag{8.121}$$

These expressions for w_2 and its derivative are substituted into the original differential equation

$$-Ak_2 e^{k_2 t} - Bk_1 e^{-k_1 t} + k_2 Ae^{-k_2 t} + k_2 Be^{-k_1 t} = k_1 b_{21} m_1(0)e^{-k_1 t} \tag{8.122}$$

which simplifies to

$$(-k_1 B + k_2 B)e^{-k_1 t} = k_1 b_{21} m_1(0) e^{-k_1 t} \tag{8.123}$$

so that B is given by

$$B = \frac{k_1 b_{21} m_1(0)}{k_2 - k_1} \tag{8.124}$$

A must be evaluated from the initial condition.

$$m_2(0) = A + B \tag{8.125}$$

which gives

$$A = m_2(0) - B \tag{8.126}$$

and

$$\begin{aligned} m_2 &= m_2(0)e^{-k_2 t} - B(e^{-k_2 t} - e^{-k_1 t}) \\ &= m_2(0)e^{-k_2 t} - \frac{k_1 b_{21} m_1(0)}{k_2 - k_1}(e^{-k_2 t} - e^{-k_1 t}) \end{aligned} \tag{8.127}$$

The solution can be continued in this way to develop the solution from size to size. The solution is tedious but not impossible. It is better to develop a solution that works automatically for all sizes and which is especially suited to computer methods of solution. Note firstly that a general solution can take two forms:

$$\begin{aligned} m_i &= \sum_{j=1}^{i} \alpha_{ij} e^{-k_j t} \\ m_i &= \sum_{j=1}^{i} \beta_{ij} m_j(0) \end{aligned} \tag{8.128}$$

The coefficients α_{ij} are not functions of time but are functions of the initial conditions and the coefficients β_{ij} are not functions of the initial conditions but they vary with the time. The coefficients α_{ij} can be developed through some recursion relationships as follows:
The differential equation that describes the variation of each of the size classes is

$$\frac{dm_i}{dt} = -k_i m_i + \sum_{j=1}^{i-1} b_{ij} k_j m_j \tag{8.129}$$

The general solution is now substituted into this equation

$$\sum_{j=1}^{i} -\alpha_{ij} k_j e^{k_j t} = -k_i \sum_{j=1}^{i} \alpha_{ij} e^{-k_j t} + \sum_{j=1}^{i-1} b_{ij} k_j \sum_{l=1}^{j} \alpha_{jl} e^{-k_l t} \tag{8.130}$$

Re-arranging and collecting terms

$$\sum_{j=1}^{i} \alpha_{ij}(k_i - k_j)e^{-k_j t} = \sum_{j=1}^{i-1}\sum_{l=1}^{j} b_{ij}k_j\alpha_{jl}e^{-k_l t} \tag{8.131}$$

The order of the double summation must now be reversed

$$\sum_{l=1}^{i-1} \alpha_{il}(k_i - k_l)e^{-k_l t} = \sum_{l=1}^{i-1}\sum_{j=l}^{i-1} b_{ij}k_j\alpha_{jl}e^{-k_l t} \tag{8.132}$$

The change in the limits on the double summation should be noted particularly, The region over which the double summation operates must not change as the order of summation is switched.
Now the terms are collected

$$\sum_{l=1}^{i-1}\left(\alpha_{il}(k_i - k_l) - \sum_{j=l}^{i-l} b_{ij}k_j\alpha_{jl}\right)e^{-k_l t} = 0 \tag{8.133}$$

The coefficient of each exponential must be zero if the summation is to be zero for every value of *t*.

$$\alpha_{il}(k_i - k_l) = \sum_{j=l}^{i-1} b_{ij}k_j\alpha_{jl} \tag{8.134}$$

which provides the value of each value of α except for α_{ii}.

$$\alpha_{il} = \frac{1}{k_i - k_l}\sum_{j=l}^{i-1} b_{ij}k_j\alpha_{jl} \qquad for\ i>l \tag{8.135}$$

α_{ii} can be obtained from the initial condition

$$m_i(0) = \sum_{j=1}^{i} \alpha_{ij} = \alpha_{ii} + \sum_{j=1}^{i-1} \alpha_{ij} \tag{8.136}$$

$$\alpha_{ii} = m_i(0) - \sum_{j=1}^{i-1} \alpha_{ij} \tag{8.137}$$

All the coefficients can be solved by recursion *starting from i=1*.

$$\begin{aligned} \alpha_{11} &= m_1(0) \\ \alpha_{21} &= \frac{1}{k_2 - k_1}b_{21}k_1\alpha_{11} \end{aligned} \tag{8.138}$$

etc.
This recursion is most useful in the form

$$\alpha_{ij} = c_{ij}a_j \quad \text{with } j<i \quad \text{and } c_{ii} = 1 \tag{8.139}$$

$$\alpha_{il} = c_{il} a_l = \frac{1}{k_i - k_l} \sum_{j=l}^{i-1} b_{ij} k_j c_{jl} a_l$$
$$c_{il} = \frac{1}{k_i - k_l} \sum_{j=l}^{i-1} b_{ij} k_j c_{jl} \qquad (8.140)$$

$$\alpha_{ii} = a_i = m_{i(0)} - \sum_{j=1}^{i-1} c_{ij} a_j \qquad (8.141)$$

Then the c_{il}'s are independent of both the time and the initial conditions and they can be calculated once and for all from a knowledge of the specific breakage rate constants and the breakage function.

8.10.2 Batch grinding of heterogeneous solids

The batch comminution equation for heterogeneous solids is

$$\frac{dp_{ij}}{dt} = -S_{ij} p_{ij} + \sum_{l=1}^{j-1} \sum_{k=K_l^*}^{K_l^{**}} S_{kl} b_{ijkl} p_{kl} \qquad (8.142)$$

In equation (8.142) *i,j,k* and *l* index the parent particle composition, the parent size, the progeny composition and the progeny size respectively. K_l^* and K_l^{**} are the left and right hand boundaries of region R' in the Andrews-Mika diagram for parent particles in size class *l*. b_{ijkl} is the discretized version of the function $b(g,D|g',D')$.

In practice it is convenient to decouple the size reduction process from the liberation process. This can be done by using the conditional breakage functions

$$b_{ijkl} = b_{j,kl}\ b_{i,jkl} \qquad (8.143)$$

where $b_{j,kl}$ is the fraction of material breaking from class *k,l* that reports to size class *j*. $b_{i,jkl}$ is the conditional transfer coefficient from grade class *k* to grade class *i* given that the particle transfers from size class *l* to size class *j*. $b_{i,jkl}$ is usually represented as an Andrews-Mika diagram. We refer to $b_{j,kl}$ as the "size breakage function" and $b_{i,jkl}$ as the Andrews-Mika coefficients. Equation (8.143, 8.143) is completely general and does not depend on the assumption of random fracture. $b_{j,kl}$ and $b_{i,jkl}$ are conditional distributions and must satisfy the conditions

$$\sum_{j=l+1}^{N} b_{j,kl} = 1 \qquad (8.144)$$

and

$$\sum_{i=1}^{12} b_{i,jkl} = 1 \qquad (8.145)$$

Typical examples of the discretized Andrews-Mika diagram are shown in Figures 8.24 and 8.25. It is important to realize that these represent just two of the many discrete Andrews-Mika diagrams that are required to characterize any

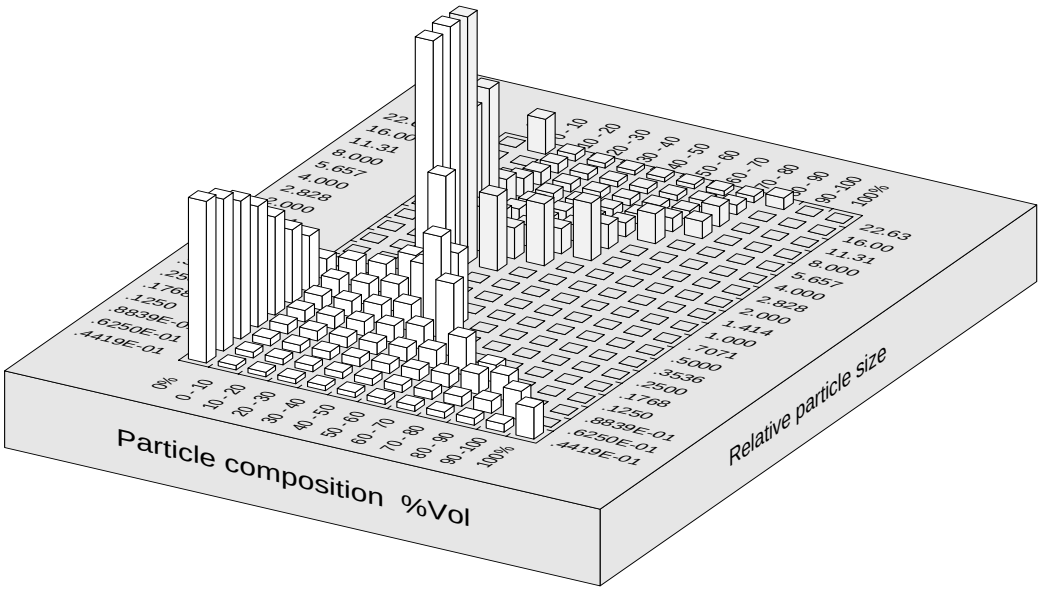

Figure 8.24 Internal structure of a typical Andrews-Mika diagram showing both the feeder and attainable regions. The feeder region is indicated by the shaded bars in the upper half of the diagram and the attainable region is indicated by the unshaded bars in the lower half of the diagram. The height of each bar in the feeder region represents the conditional multi-component breakage function $b_{4,10kl}$ where k and l represent any parent bar in the feeder region. The height of each bar in the attainable region represents the value of $a_{m,n\,4\,10}$.

particular ore. Figures 2 and 3 show a discretization over 19 size classes and 12 grade classes which requires 19×12 = 228 separate Andrews-Mika diagrams, one for each possible combination of *k* and *l*. In general a theoretical model of the Andrews-Mika diagram is required to generate the appropriate matrices which can be stored before the solution to the batch comminution equation is generated. Appropriate models for the Andrews-Mika diagram are discussed in Chapter 3.

A solution to the heterogeneous batch comminution equation can be generated by exploiting the linearity of the differential equations to generate the general solution

$$p_{ij} = \sum_{l=1}^{j} \sum_{k=1}^{12} \alpha_{ijkl} e^{-S_{kl} t} \tag{8.146}$$

The coefficients in equation (8.146) are related to the selection and breakage functions and to the initial conditions using the following recursion relationships

$$\alpha_{ijmj} = 0 \qquad \text{if } i \neq m \tag{8.147}$$

$$\alpha_{ijij} = p_{ij}(0) - \sum_{l=1}^{j-1} \sum_{k=1}^{12} \alpha_{ijkl} \tag{8.148}$$

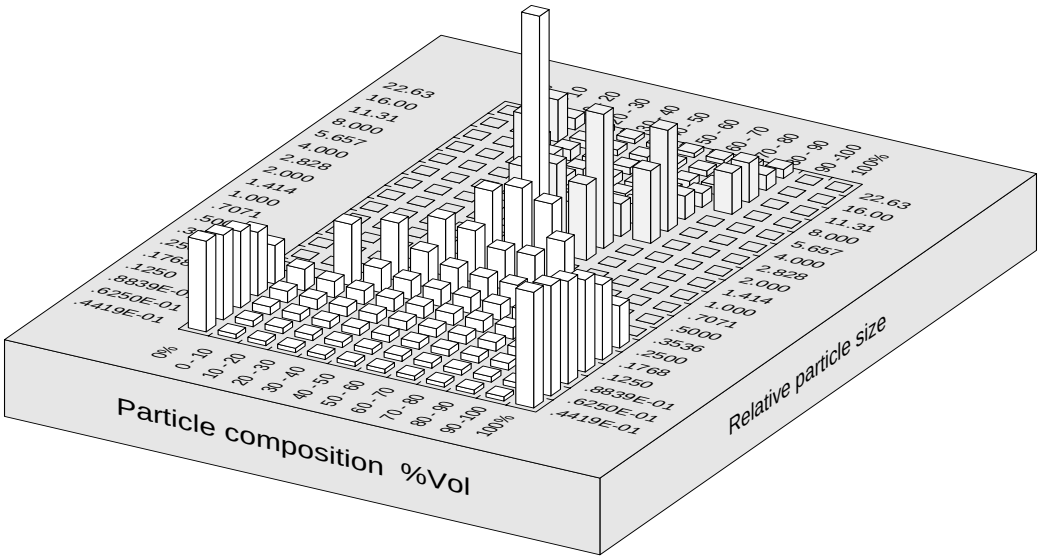

Figure 8.25 Internal structure of a typical Andrews-Mika diagram showing both the feeder and attainable regions. The feeder region is indicated by the shaded bars in the upper half of the diagram and the attainable region is indicated by the unshaded bars in the lower half of the diagram. The height of each bar in the feeder region represents the conditional multi-component breakage function $b_{7,10kl}$ where k and l represent any parent bar in the feeder region. The height of each bar in the attainable region represents the value of $a_{m,n\ 7\ 10}$.

$$\alpha_{ijmn} = \frac{\sum_{l=n}^{j-1} \sum_{k=1}^{12} S_{kl}\, b_{ijkl} \alpha_{klmn}}{S_{ij} - S_{mn}} \qquad (8.149)$$

Note that the summations in equation (8.149) run over the feeder regions and not over the attainable regions.

This solution to equation (8.142) is based on the usual convention that breakage implies that all progeny leave the size class of the parent particle. The pathological case $S_{ij} = S_{mn}$ is occasionally encountered in practice. When it occurs, it is usually handled by making a slight adjustment to the parameters that define the relationship between the specific rate of breakage and the particle size to assure that no two values of S_{ij} are exactly equal.

Equation (8.146) represents a complete and convenient solution to the discrete version of the batch comminution equation with liberation and this solution produces the size distribution as well as the liberation distribution as a function of the time of grinding.